Intermittency and geometrical statistics of three-dimensional homogeneous magnetohydrodynamic turbulence: A wavelet viewpoint

Katsunori Yoshimatsu,[1,a)] Kai Schneider,[2,b)] Naoya Okamoto,[3] Yasuhiro Kawahara,[1] and Marie Farge[4]
[1]*Department of Computational Science and Engineering, Nagoya University, Nagoya 464-8603, Japan*
[2]*M2P2–CNRS & CMI, Université de Provence, 39 rue Frédéric Joliot-Curie, 13453 Marseille Cedex 13, France*
[3]*Center for Computational Science, Graduate School of Engineering, Nagoya University, Nagoya 464-8603, Japan*
[4]*LMD–IPSL–CNRS, Ecole Normale Supérieure, 24 rue Lhomond, 75231 Paris Cedex 05, France*

(Received 13 May 2011; accepted 5 August 2011; published online 9 September 2011)

Scale-dependent and geometrical statistics of three-dimensional incompressible homogeneous magnetohydrodynamic turbulence without mean magnetic field are examined by means of the orthogonal wavelet decomposition. The flow is computed by direct numerical simulation with a Fourier spectral method at resolution 512^3 and a unit magnetic Prandtl number. Scale-dependent second and higher order statistics of the velocity and magnetic fields allow to quantify their intermittency in terms of spatial fluctuations of the energy spectra, the flatness, and the probability distribution functions at different scales. Different scale-dependent relative helicities, e.g., kinetic, cross, and magnetic relative helicities, yield geometrical information on alignment between the different scale-dependent fields. At each scale, the alignment between the velocity and magnetic field is found to be more pronounced than the other alignments considered here, i.e., the scale-dependent alignment between the velocity and vorticity, the scale-dependent alignment between the magnetic field and its vector potential, and the scale-dependent alignment between the magnetic field and the current density. Finally, statistical scale-dependent analyses of both Eulerian and Lagrangian accelerations and the corresponding time-derivatives of the magnetic field are performed. It is found that the Lagrangian acceleration does not exhibit substantially stronger intermittency compared to the Eulerian acceleration, in contrast to hydrodynamic turbulence where the Lagrangian acceleration shows much stronger intermittency than the Eulerian acceleration. The Eulerian time-derivative of the magnetic field is more intermittent than the Lagrangian time-derivative of the magnetic field.
 [doi:10.1063/1.3628637]

I. INTRODUCTION

Magnetohydrodynamic (MHD) turbulence is encountered in a variety of applications going from astrophysics,[1,2] e.g., the solar wind, to engineering, e.g., liquid metals in dynamo experiments.[3–5] MHD turbulence is characterized by its wide range of dynamically active scales together with strong intermittency. The magnetic field coupled with the conducting fluid induces various dynamics; e.g., pronounced alignment or anti-alignment between the magnetic and velocity fields, so-called dynamic alignment (see, e.g., Refs. 6–17), and nonlinear interactions between the magnetic and the velocity field; for a recent review on the interactions, we refer to Ref. 18. MHD turbulence can exhibit small-scale intermittency whose type differs from what is observed in hydrodynamic (HD) turbulence.

Intermittency of MHD turbulence is attributed to coherent structures,[19] as first suggested by Batchelor and Townsend[20] for HD turbulence. For a given flow realization, the structures are inhomogeneously distributed in space and time. The flow intermittency is typically reflected by the power law exponents of the p-th order structure functions of velocity in HD turbulence (see, e.g., Ref. 21) and those of the Elsässer variables, velocity, and magnetic field for MHD turbulence (see, e.g., Refs. 22–24). In Refs. 25 and 26, Homann *et al*. showed that the Eulerian velocity in MHD turbulence is more intermittent than in HD turbulence, whereas the situation is reversed for the Lagrangian velocity. The magnetic field is even more intermittent than the velocity field.[27,28] In Ref. 17, it was suggested that local alignment or anti-alignment of the velocity and the magnetic field is a robust process which leads to spatial intermittency through the weakening of nonlinear interactions.

In the present paper, we address the question: what are similarities and differences of small-scale intermittency in HD and MHD turbulence? To answer this, we here use and generalize the diagnostics introduced in Ref. 29, which are based on the orthonormal wavelet decomposition. Therein, different wavelet based tools to examine scale-dependent statistics of fully developed three-dimensional (3D) HD turbulence were proposed. It was shown that the scale-dependent velocity flatness quantifies the spatial variability of the energy spectrum and exhibits a substantial increase at small scales. By

[a)]Electronic mail: yosimatu@fluid.cse.nagoya-u.ac.jp.
[b)]Electronic mail: kschneid@cmi.univ-mrs.fr.

introducing the scale-dependent kinetic helicity, the geometrical statistics of the flow were quantified. Statistical scale-dependent analyses of both of the Eulerian and the Lagrangian acceleration confirmed their different intermittency.

Orthonormal wavelets yield a suitable multiscale representation of intermittent fields, because they take the lacunarity of the small-scale activity into account and provide a clear scale-separation. The wavelet transform decomposes a given flow field into well-localized scale-space contributions, thus allows for a sparse representation of intermittent data and permits to quantify the degree of intermittency at different scales. The p-th order scale-dependent moment of an intermittent field is related to the structure function of the field (see, e.g., Ref. 30). Compared to the increments of the structure functions, wavelets typically have more than one vanishing moment and can thus overcome the limitations of structure functions, e.g., they can detect steeper power law behaviors. Wavelet methodologies have been developed for HD turbulence since the pioneering work.[31–33] Readers interested in a recent review of application of wavelets to turbulence may refer to Ref. 34. In Ref. 35, it was shown that the wavelet representation of 3D MHD turbulence is efficient with respect to the number of required modes to represent the coherent vorticity sheets and current sheets.

The remainder of the paper is organized as follows. First, in Sec. II, we briefly describe the tools to perform scale-dependent statistics using the orthogonal wavelet decomposition. Then, in Sec. III, we describe the direct numerical simulation (DNS) of 3D incompressible homogeneous MHD turbulence without mean magnetic field. Section IV presents the numerical results of MHD turbulence. We analyze velocity and magnetic fields and study different relative scale-dependent helicities, e.g., relative scale-dependent kinetic, cross, and magnetic helicities. The Eulerian and Lagrangian accelerations together with their analogous quantities, the partial and total time-derivatives of the magnetic field, are also investigated. The results about the kinetic helicity and the accelerations are compared with those for 3D homogeneous isotropic HD turbulence. Finally, some conclusions are drawn in Sec. V.

II. ORTHOGONAL WAVELET ANALYSIS AND SCALE-DEPENDENT STATISTICS

The goal of this section is to summarize briefly the wavelet tools to perform scale-dependent statistics and to define all used quantities in a concise and self-consistent way. In the following, we consider a generic vector valued quantity $\boldsymbol{v}(\boldsymbol{x})$ which stands either for velocity $\boldsymbol{u}$ or the magnetic field $\boldsymbol{b}$. The field $\boldsymbol{b}$ is normalized by $(\mu_0\rho_0)^{1/2}$, where μ_0 is the permeability of free space and ρ_0 is the fluid density. The introduced concepts can also be applied to the derived quantities like vorticity $\boldsymbol{\omega}=\nabla\times\boldsymbol{u}$ or the current density $\boldsymbol{j}=\nabla\times\boldsymbol{b}$.

A. Vector valued orthogonal wavelet decomposition

The starting point is a 3D 2π-periodic vector field $\boldsymbol{v}(\boldsymbol{x})=(v^1(\boldsymbol{x}), v^2(\boldsymbol{x}), v^3(\boldsymbol{x}))$ with $\boldsymbol{x}=(x^1,x^2,x^3)\in\Omega=[0,2\pi]^3\subset\mathbb{R}^3$ and $v^\ell\in L^2(\Omega)$ $(\ell=1, 2, 3)$ sampled on $N=2^{3J}$ equidistant grid points. The number of octaves in each space direction of the Cartesian coordinate is denoted by J. The 3D orthonormal wavelet transform unfolds $\boldsymbol{v}$ into scale, positions, and seven directions using a 3D mother wavelet $\psi_\mu(\boldsymbol{x})$, which is based on a tensor product construction.

The wavelet is well-localized in space $\boldsymbol{x}$, oscillating, and smooth. The mother wavelet generates a family of wavelets $\psi_{\mu,\lambda}(\boldsymbol{x})$ by dilation and translation, which yields an orthogonal basis of $L^2(\mathbb{R}^3)$ and also of $L^2(\Omega)$ through the application of a periodization technique.[36] The spatial average of $\psi_{\mu,\lambda}(\boldsymbol{x})$, denoted by $\langle\psi_{\mu,\lambda}\rangle$, vanishes for each index. Here, the multi-index $\lambda=(j, i_1, i_2, i_3)$ denotes the scale 2^{-j} and the position $2^{-j}\boldsymbol{i}=2^{-j}(i_1, i_2, i_3)$ of the wavelets for each direction $\mu=1,\ldots,7$.

The vector field $\boldsymbol{v}$, having a mean value $\langle\boldsymbol{v}\rangle$ (which vanishes in the present applications for all components), can be decomposed into an orthogonal wavelet series

$$\boldsymbol{v}(\boldsymbol{x})=\langle\boldsymbol{v}\rangle+\sum_{j=0}^{J-1}\boldsymbol{v}_j(\boldsymbol{x}), \tag{1}$$

where $\boldsymbol{v}_j$ is the contribution of $\boldsymbol{v}$ at scale 2^{-j} defined by

$$\boldsymbol{v}_j(\boldsymbol{x})=\sum_{\mu=1}^{7}\sum_{i_1,i_2,i_3=0}^{2^j-1}\tilde{\boldsymbol{v}}_{\mu,\lambda}\psi_{\mu,\lambda}(\boldsymbol{x}). \tag{2}$$

Due to orthogonality of the wavelets, the coefficients are given by $\tilde{\boldsymbol{v}}_{\mu,\lambda}=\langle\boldsymbol{v},\psi_{\mu,\lambda}\rangle$, where $\langle\cdot,\cdot\rangle$ denotes the L^2-inner product defined by $\langle f,g\rangle=\int_\Omega f(\boldsymbol{x})g(\boldsymbol{x})d\boldsymbol{x}$. Note that $\langle\boldsymbol{v}_j\rangle=\boldsymbol{0}$. At scale 2^{-j}, we have 7×2^{3j} wavelet coefficients. The N coefficients, which consist of $N-1$ wavelet coefficients $\tilde{\boldsymbol{v}}_{\mu,\lambda}$ and the mean value $\langle\boldsymbol{v}\rangle$, are efficiently computed from the N grid point values of $\boldsymbol{v}$ by the use of the fast wavelet transform which has linear complexity. For more details on wavelets, we refer the reader to text books, e.g., Mallat.[36]

B. Scale-dependent statistics

1. Energy spectra, spatial fluctuations, and scale-dependent flatness

From the scale-dependent energy of $\boldsymbol{v}$ defined as $e_j^v=\langle\boldsymbol{v}_j,\boldsymbol{v}_j\rangle/2$, the total energy $\bar{E}^v=\sum_{j=0}^{J-1}e_j^v$ is recovered thanks to the scale orthogonality. The scale 2^{-j} can be related to the wavenumber k_j by $k_j=k_\psi 2^j$, where k_ψ is the centroid wavenumber of the chosen wavelet ($k_\psi=0.77$ for the Coiflet 12 used here). Therewith, the component averaged wavelet energy spectrum of $\boldsymbol{v}$ can be defined as

$$\tilde{E}_j^v=\frac{1}{\Delta k_j}\langle e_j^{v,\ell}\rangle_c, \tag{3}$$

where $\langle\cdot\rangle_c=\sum_{\ell=1}^{3}\langle\cdot\rangle/3$, $e_j^{v,\ell}=(v_j^\ell)^2/2$, v_j^ℓ is the ℓ-th component of $\boldsymbol{v}_j$ and $\Delta k_j=k_j\ln 2$. The variable v denotes either u or b for velocity $\boldsymbol{u}$ or magnetic field $\boldsymbol{b}$, respectively. We average here over all components of $\boldsymbol{v}$, because in Sec. IV, we consider 3D homogeneous MHD turbulence without mean magnetic field as well as 3D homogeneous isotropic HD turbulence. Note that the wavelet spectrum $\tilde{E}_j^v$ corresponds to a smoothed version of the Fourier energy spectrum.[31,32]

We can then quantify the spatial variability of the energy spectrum at a given wavenumber k_j as the standard deviation of $\tilde{E}_j^v$ defined by

$$\tilde{\sigma}_j^v = \frac{1}{\Delta k_j}\sqrt{\langle (e_j^{v,\ell})^2\rangle_c - (\langle e_j^{v,\ell}\rangle_c)^2}. \tag{4}$$

To study higher order scale-dependent statistics, we define the scale-dependent flatness of the vector $\boldsymbol{v}$ by

$$F[\boldsymbol{v}_j] = \frac{\langle (v_j^\ell)^4\rangle_c}{\{\langle (v_j^\ell)^2\rangle_c\}^2}, \tag{5}$$

noting that $\langle v_j^\ell\rangle = 0$. This quantity can be expressed in terms of the wavelet energy spectrum (Eq. (3)) and its standard deviation (Eq. (4)) by the relation:[37]

$$F[\boldsymbol{v}_j] = \left(\frac{\tilde{\sigma}_j^v}{\tilde{E}_j^v}\right)^2 + 1. \tag{6}$$

2. Scale-dependent helicities

The kinetic helicity, defined as $H^{\mathrm{K}}(\boldsymbol{x}) = \boldsymbol{u}\cdot\boldsymbol{\omega}$, yields a quantitative measure of the geometrical statistics of turbulence. The statistics of isotropic turbulence and their relevance to structures have been examined since the late 1980s, for example, in Refs. 38–40. For a review, we refer to Ref. 41. To get insight into the scale-dependent geometrical statistics, the scale-dependent kinetic helicity defined by

$$H_j^{\mathrm{K}}(\boldsymbol{x}) = \boldsymbol{u}_j\cdot\boldsymbol{\omega}_j \tag{7}$$

was introduced.[29] The scale-dependent kinetic helicity H_j^{K} preserves Galilean invariance, though kinetic helicity $\boldsymbol{u}\cdot\boldsymbol{\omega}$ itself does not.

In ideal MHD turbulence, the mean cross helicity, defined as $\bar{H}^{\mathrm{C}} = \langle \boldsymbol{u}\cdot\boldsymbol{b}\rangle$, and the mean magnetic helicity, defined as $\bar{H}^{\mathrm{M}} = \langle \boldsymbol{a}\cdot\boldsymbol{b}\rangle$, are conserved quantities. Here, $\boldsymbol{a}$ is the vector potential of the magnetic field $\boldsymbol{b}$, where $\nabla\cdot\boldsymbol{a} = 0$ and $\langle \boldsymbol{a}\rangle = \boldsymbol{0}$. The scale-dependent cross helicity and the magnetic helicity can be defined by

$$H_j^{\mathrm{C}}(\boldsymbol{x}) = \boldsymbol{u}_j\cdot\boldsymbol{b}_j, \tag{8}$$

$$H_j^{\mathrm{M}}(\boldsymbol{x}) = \boldsymbol{a}_j\cdot\boldsymbol{b}_j, \tag{9}$$

respectively. Then, the scale-dependent "super-magnetic helicity" is defined as

$$H_j^{\mathrm{SM}}(\boldsymbol{x}) = \boldsymbol{b}_j\cdot\boldsymbol{j}_j. \tag{10}$$

The nomenclature is based on the study on HD turbulence,[42] where the helicity of vorticity defined by $\boldsymbol{\omega}\cdot(\nabla\times\boldsymbol{\omega})$ is called "super helicity."

The corresponding mean helicities are obtained by summation over scale, $\bar{H}^\alpha = \sum_j \langle H_j^\alpha\rangle$ (α = K, C, M, SM), thanks to the orthogonality of the wavelet. Their scale-dependent relative helicities can be defined by

$$h_j^{\mathrm{K}}(\boldsymbol{x}) = \frac{H_j^{\mathrm{K}}}{|\boldsymbol{u}_j||\boldsymbol{\omega}_j|}, \tag{11}$$

$$h_j^{\mathrm{C}}(\boldsymbol{x}) = \frac{H_j^{\mathrm{C}}}{|\boldsymbol{u}_j||\boldsymbol{b}_j|}, \tag{12}$$

$$h_j^{\mathrm{M}}(\boldsymbol{x}) = \frac{H_j^{\mathrm{M}}}{|\boldsymbol{a}_j||\boldsymbol{b}_j|}, \tag{13}$$

$$h_j^{\mathrm{SM}}(\boldsymbol{x}) = \frac{H_j^{\mathrm{SM}}}{|\boldsymbol{b}_j||\boldsymbol{j}_j|}. \tag{14}$$

These quantities define the cosine of the angle between two vectors, e.g., $\boldsymbol{u}$ and $\boldsymbol{\omega}$, at each spatial grid point and thus their ranges lie between -1 and $+1$.

III. DNS OF MHD TURBULENCE

We performed DNS of forced 3D incompressible MHD turbulence without mean magnetic field in a 2π periodic box Ω. The flow obeys the following equations:

$$\partial_t\boldsymbol{u} + (\boldsymbol{u}\cdot\nabla)\boldsymbol{u} = -\frac{1}{\rho_0}\nabla P + \boldsymbol{j}\times\boldsymbol{b} + \nu\Delta\boldsymbol{u} + \boldsymbol{f}, \tag{15}$$

$$\partial_t\boldsymbol{b} + (\boldsymbol{u}\cdot\nabla)\boldsymbol{b} = (\boldsymbol{b}\cdot\nabla)\boldsymbol{u} + \eta\Delta\boldsymbol{b}, \tag{16}$$

$$\nabla\cdot\boldsymbol{u} = 0, \tag{17}$$

$$\nabla\cdot\boldsymbol{b} = 0, \tag{18}$$

where t is time, $\boldsymbol{f}$ is an external force, P is the pressure, ν is the kinematic viscosity, η is the magnetic diffusivity, and $\partial_t = \partial/\partial t$. The Prandtl number Pr is set to 1, i.e., $\eta = \nu$.

The above equations are computed with a Fourier pseudo-spectral method at $N = 512^3$ ($J = 9$) grid points. The aliasing errors are removed by means of the phase shift method. Only modes with wavenumbers satisfying $k < 2^{1/2}N^{1/3}/3$ are retained, where $k = |\boldsymbol{k}|$, $\boldsymbol{k}$ is a wave vector and $N^{1/3}$ is the number of grid points in each direction of the Cartesian coordinate. A fourth-order Runge-Kutta method is used for time integration. The time increment Δt is set to $\Delta t = 1.5\times10^{-3}$ and $\nu = \eta = 3.6\times10^{-4}$. We imposed a solenoidal random force with a correlation time 3.0 and an intensity 0.9×10^{-3}, only in the wavenumber range $1 \le k < 2.5$. Readers interested in details of how to generate such random forces are referred to the Appendix of Ref. 43. The initial velocity and magnetic fields are given by linear superposition of random fields and deterministic fields. The random fields are generated under the constraints, $E^u(k) = E^b(k) = C_1k^4\exp(-k^2/8)$, where $E^u(k)$ and $E^b(k)$ are the kinetic and magnetic energy spectra, respectively. The deterministic fields are given by $\boldsymbol{u} = \boldsymbol{L}(0.5, 2)$ and $\boldsymbol{b} = \boldsymbol{L}^b(0.6, 1)$, where $\boldsymbol{L}^u(C_0, \kappa) = C_0(\sin(\kappa z) + \cos(\kappa y), \sin(\kappa x) + \cos(\kappa z), \sin(\kappa y) + \cos(\kappa x))$. The constant C_1 is determined so that the total kinetic and the magnetic energy satisfy $\bar{E}^u = \bar{E}^b = 0.5$. The initial mean cross helicity $\bar{H}^{\mathrm{C}}$ is almost zero, $\bar{H}^{\mathrm{C}} = 3.78\times10^{-2}$, and the mean magnetic helicity $\bar{H}^{\mathrm{M}}$ is set to $\bar{H}^{\mathrm{M}} = 0.515$. The normalized mean helicities have the values $\mathcal{H}^{\mathrm{C}} = 3.78\times10^{-2}$ and $\mathcal{H}^{\mathrm{M}} = 0.691$, where, $\mathcal{H}^{\mathrm{C}} = \bar{H}^{\mathrm{C}}/\{2(\bar{E}^u\bar{E}^b)^{1/2}\}$ and $\mathcal{H}^{\mathrm{M}} = \bar{H}^{\mathrm{M}}/(2\bar{E}^b\langle|\boldsymbol{a}|^2\rangle)^{1/2}$.

The simulation is performed up to $t = 9(\sim 5.9T_i)$ when the energy dissipation rate per unit mass $\langle\epsilon\rangle$ remains almost constant, which characterizes the behavior of small scales

TABLE I. Characteristics of the DNS at the final time for MHD turbulence. The normalized mean helicities are given as $\mathcal{H}^{\mathrm{K}} = 0.909 \times 10^{-3}$, $\mathcal{H}^{\mathrm{C}} = -7.52 \times 10^{-3}$, and $\mathcal{H}^{\mathrm{M}} = 0.655$, where $\mathcal{H}^{\mathrm{K}} = \bar{H}^{\mathrm{K}}/(2\bar{E}^u\langle|\boldsymbol{\omega}|^2\rangle)^{1/2}$.

$\bar{E}^u$	$\bar{E}^b$	$\bar{H}^{\mathrm{K}}(\times 10^{-3})$	$\bar{H}^{\mathrm{C}}(\times 10^{-3})$	$\bar{H}^{\mathrm{M}}$	$\eta_{\mathrm{IK}}(\times 10^{-3})$	R^u_λ	R^b_λ
0.238	0.618	7.16	−5.77	0.503	8.79	150	306

and thus corresponds to a statistically quasi-stationary state. Here, T_i is the initial large eddy turnover time defined by $T_i = L^u/u_0$, where $u_0 = (2\bar{E}^u/3)^{1/2}$, L^u is the integral length scale given by $L^u = \pi/(2u_0^2)\int_0^{k_{\max}} \mathrm{d}k\, E^u(k)/k$, and $k_{\max}$ is the maximum wave number. The absolute value of the total cross helicity remains below 4.0×10^{-2} during the whole computation. The characteristics of the DNS at the final time are provided in Table I. The Iroshnikov and Kraichnan microscale η_{IK} is defined by $(\nu^2 b_0/\langle\epsilon\rangle)^{1/3}$, where $b_0 = (2\bar{E}^b/3)^{1/2}$. The kinetic and magnetic Taylor microscale Reynolds numbers are given by $R^u_\lambda = u_0\lambda^u/\nu$ and $R^b_\lambda = b_0\lambda^b/\eta$, respectively, where the kinetic Taylor microscale $\lambda^u = (15\nu u_0^2/\langle\epsilon^u\rangle)^{1/2}$ and the magnetic Taylor microscale $\lambda^b = (15\eta b_0^2/\langle\epsilon^b\rangle)^{1/2}$. Here, $\langle\epsilon^u\rangle$ and $\langle\epsilon^b\rangle$ are the kinetic and magnetic energy dissipation rates, respectively, and $\langle\epsilon\rangle = \langle\epsilon^u\rangle + \langle\epsilon^b\rangle$.

IV. NUMERICAL RESULTS

We apply the scale-dependent statistics presented in Sec. II to the DNS data of MHD turbulence. We also use the DNS data of 3D incompressible HD turbulence at $R^u_\lambda = 173$ with $k_{\max}\eta_{\mathrm{K}} = 2$, which was computed at 512^3 grid points, for details we refer to Refs. 44 and 45, in order to compare qualitatively the statistics of MHD with those of HD, especially in terms of the relative scale-dependent kinetic helicity and the accelerations. Here, η_{K} is the Kolmogorov length scale defined as $\eta_{\mathrm{K}} = (\nu^3/\langle\epsilon^u\rangle)^{1/4}$.

A. Energy spectra and spatial fluctuations

First the scale-distributions of the second-order moments of velocity and magnetic field, which correspond to kinetic and magnetic energies, respectively, are studied. Figure 1 shows the wavelet kinetic and magnetic energy spectra, $\tilde{E}^u_j$ and $\tilde{E}^b_j$, and the corresponding spatial variabilities, $\tilde{\sigma}^u_j$ and $\tilde{\sigma}^b_j$, as a function of the dimensionless wavenumber $k_j\eta_{\mathrm{IK}}(j = 0, \ldots, 8)$. In Fig. 1(a), we observe that $\tilde{E}^u_j$ and $\tilde{E}^b_j$ coincide well with the one-component Fourier kinetic and magnetic energy spectra, $E^u(k)/3$ and $E^b(k)/3$, respectively. The magnetic energy spectrum $\tilde{E}^b_j$ is larger than $\tilde{E}^u_j$ for each $k_j\eta_{\mathrm{IK}}$. In Fig. 1(b), it can be seen that $\tilde{\sigma}^b_j > \tilde{\sigma}^u_j$ for each $k_j\eta_{\mathrm{IK}}$. As reference, $\tilde{E}^u_j$, $E^u(k)/3$ and $\tilde{\sigma}^u_j$ for HD turbulence are shown in the insets of Fig. 1.

The probability density functions (PDFs) of the total velocity $\boldsymbol{u}$ and the total magnetic field $\boldsymbol{b}$, in Fig. 2, are almost Gaussian, as expected. (The PDFs of the vector field $\boldsymbol{v}$ are obtained by using its three components $\boldsymbol{v}^1$, $\boldsymbol{v}^2$, and $\boldsymbol{v}^3$.) The PDFs of the scale-dependent velocity $\boldsymbol{u}_j$ and magnetic field $\boldsymbol{b}_j$ exhibit heavy tails. We only consider scales for $j \geq 3$, i.e., $k_j\eta_{\mathrm{IK}} \sim 0.054$, because we are interested in the small-scale statistics. For decreasing scales, i.e., j increases, the tails of the PDFs of $\boldsymbol{u}_j$ and $\boldsymbol{b}_j$ become heavier. Note that for each j, the tails of the PDFs of $\boldsymbol{b}_j$ are decaying more slowly than the tails for $\boldsymbol{u}_j$. The behavior of the tails can be characterized by the scale-dependent flatness $F[\boldsymbol{u}_j]$ and $F[\boldsymbol{b}_j]$.

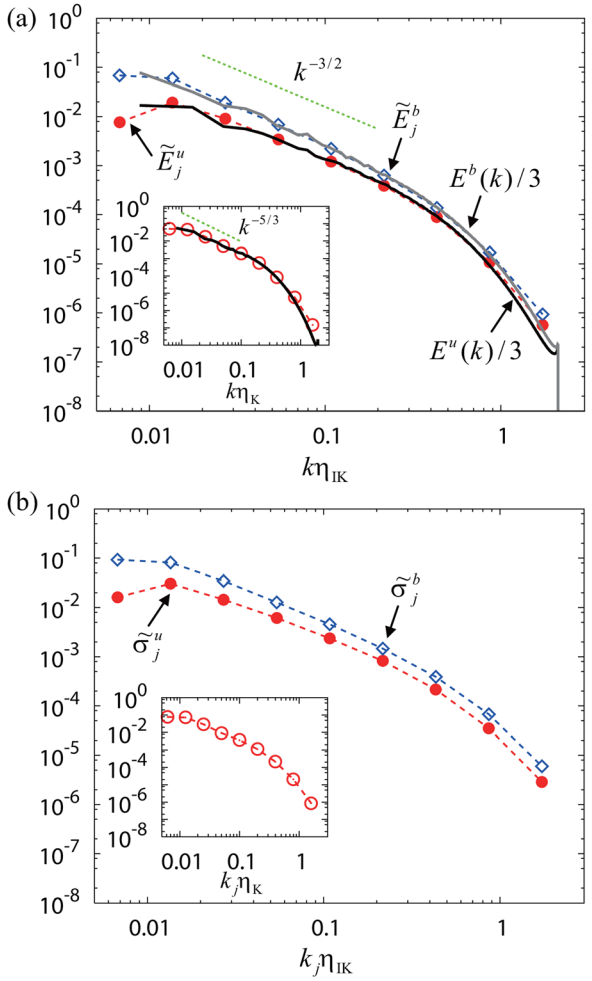

FIG. 1. (Color online) (a) Wavelet mean kinetic and magnetic energy spectra, $\tilde{E}^u_j$ and $\tilde{E}^b_j$, vs. $k\eta_{\mathrm{IK}}$ for MHD turbulence. The dashed curve with closed circles and the curve with open diamonds show $\tilde{E}^u_j$ and $\tilde{E}^b_j$, respectively. The thick black solid curve denotes the Fourier kinetic energy spectrum $E^u(k)/3$, while the thick gray solid curve denotes the Fourier magnetic spectrum $E^b(k)/3$. The inset in (a) shows the wavelet kinetic energy spectrum for HD turbulence, denoted by the dashed curves with open circles, together with the corresponding Fourier energy spectra. As reference, the power laws $k^{-3/2}$ and $k^{-5/3}$ are plotted in dotted lines. (b) Spatial variability of the wavelet kinetic and magnetic energy spectra, $\tilde{\sigma}^u_j$ and $\tilde{\sigma}^b_j$, vs. $k_j\eta_{\mathrm{IK}}$ for MHD turbulence. The inset in (b) shows $\tilde{\sigma}^u_j$ vs. $k_j\eta_{\mathrm{K}}$ for HD turbulence.

Figure 3 shows that both $F[\boldsymbol{u}_j]$ and $F[\boldsymbol{b}_j]$ increase as $k_j\eta_{\mathrm{IK}}$ increases, i.e., scale 2^{-j} decreases. We also observe that the flatness of the magnetic field, $F[\boldsymbol{b}_j]$, is larger than the flatness of the velocity field, $F[\boldsymbol{u}_j]$, for $k_j\eta_{\mathrm{IK}} \gtrsim 0.054$. Therefore, it is concluded that the magnetic field is more intermittent than the velocity, which is consistent with previous works.[27,28,35] For HD turbulence at $R^u_\lambda = 173$, $F[\boldsymbol{u}_j]$ also grows with decreasing scale, as observed for homogeneous isotropic HD turbulence at much higher $R^u_\lambda = 732$,[29] as well as, for rotating or stratified HD turbulence.[37]

B. Geometrical statistics: Helicities

Next, geometrical statistics of MHD are studied. We consider the statistics of spatial distributions of different relative scale-dependent kinetic, cross, and magnetic helicities,

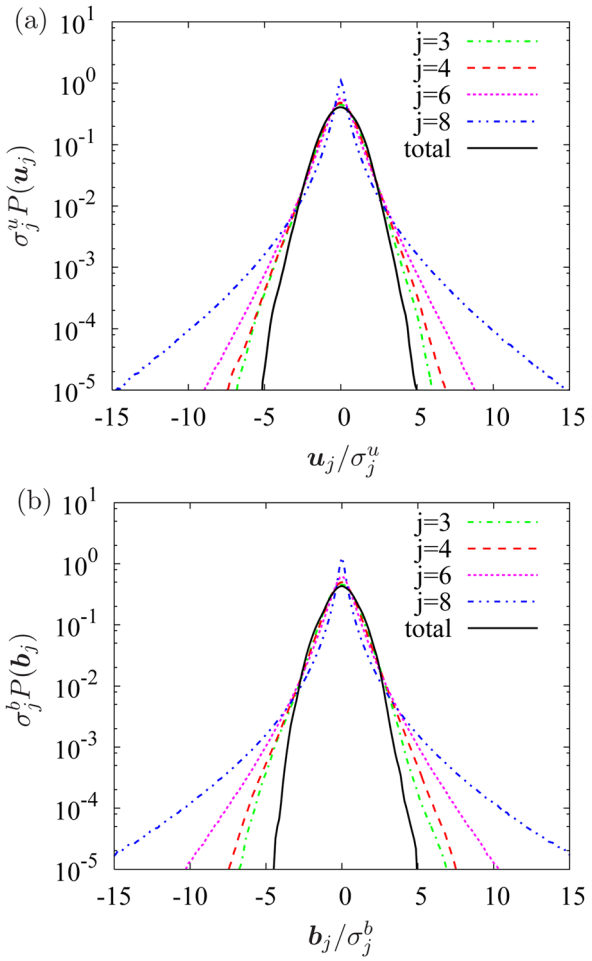

FIG. 2. (Color online) Scale-dependent PDFs of (a) velocity $\boldsymbol{u}_j$ and (b) magnetic field $\boldsymbol{b}_j$ for MHD turbulence, where σ_j^u and σ_j^b are the standard deviations of $\boldsymbol{u}_j$ and $\boldsymbol{b}_j$, respectively.

defined by Eqs. (11)–(13), respectively, together with the relative super-magnetic helicity, defined by Eq. (14).

Figure 4(a) shows two peaks in the PDF of the relative kinetic helicity $h_j^{\mathrm{K}} = \pm 1$. It can be observed that the peaks become more pronounced as $k_j\eta_{\mathrm{IK}}$ increases for the range $0.108 \lesssim k_j\eta_{\mathrm{IK}} \lesssim 0.865$ $(4 \le j \le 7)$. For $k_j\eta_{\mathrm{IK}} \sim 1.73 (j=8)$, these peaks are weaker than those at $j=7$. The peaks imply that the flow becomes more helical, i.e., scale-dependent velocity $\boldsymbol{u}_j$ becomes more aligned or anti-aligned with scale-dependent vorticity $\boldsymbol{\omega}_j$, at smaller scales except for $j=8$ where this tendency is weakened. This behavior for MHD turbulence is in contrast to the case of HD turbulence at $R_\lambda^u = 173$ shown in Fig. 4(b). The PDFs of the relative kinetic helicity present a peak for $h_j^{\mathrm{K}} = 0$ at scales $k_j\eta_{\mathrm{K}} \sim 0.050$ and 0.100 $(j=3,4)$, which corresponds to a higher probability for $\boldsymbol{u}_j$ and $\boldsymbol{\omega}_j$ be orthogonal, while at smaller scales $k_j\eta_{\mathrm{K}} \gtrsim 0.399$ $(j \ge 6)$, it has two peaks at $h_j^{\mathrm{K}} = \pm 1$. The peaks for $j \ge 6$ become more pronounced with increasing j. For HD turbulence, the behavior of h_j^{K} at $R_\lambda^u = 173$ is consistent with what was observed at much higher $R_\lambda^u = 732$ in Ref. 29. Note that the PDFs of the relative total kinetic helicities for MHD and HD turbulence, defined by $h^{\mathrm{K}}(\boldsymbol{x}) = \boldsymbol{u}\cdot\boldsymbol{\omega}/(|\boldsymbol{u}||\boldsymbol{\omega}|)$, are symmetric with respect to $h^{\mathrm{K}} = 0$ (see insets, Figs. 4(a) and 4(b)).

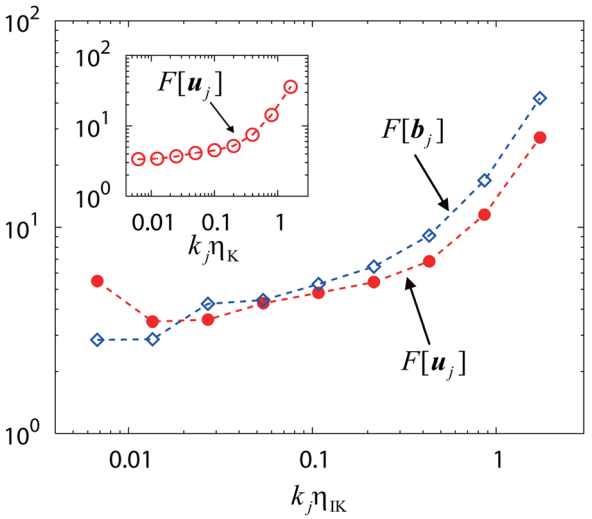

FIG. 3. (Color online) Scale-dependent flatness of velocity and magnetic field, $F[\boldsymbol{u}_j]$ and $F[\boldsymbol{b}_j]$, vs. $k_j\eta_{\mathrm{IK}}$ for MHD turbulence. The inset shows $F[\boldsymbol{u}_j]$ vs. $k_j\eta_{\mathrm{K}}$ for HD turbulence.

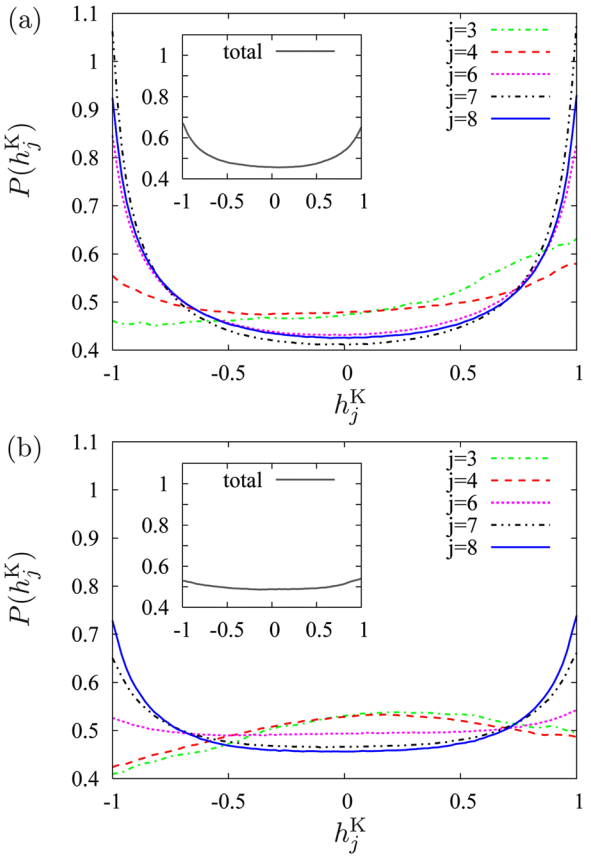

FIG. 4. (Color online) Scale-dependent PDFs of the relative kinetic helicities h_j^{K} for (a) MHD turbulence and (b) HD turbulence. The insets show the PDFs of the corresponding total relative kinetic helicities.

The PDFs of the relative scale-dependent cross helicity h_j^{C} in Fig. 5(a), have two peaks at $h_j^{\mathrm{C}} = \pm 1$, i.e., a pronounced scale-dependent dynamic alignment is found. For smaller scales, the two peaks become higher, even in the case that $\bar{H}^{\mathrm{C}} \sim 0$ and the PDF of the relative total cross helicity is symmetric (see inset, Fig. 5(a)). The higher peaks correspond to a higher probability that the scale-dependent velocity and magnetic field are aligned or anti-aligned.

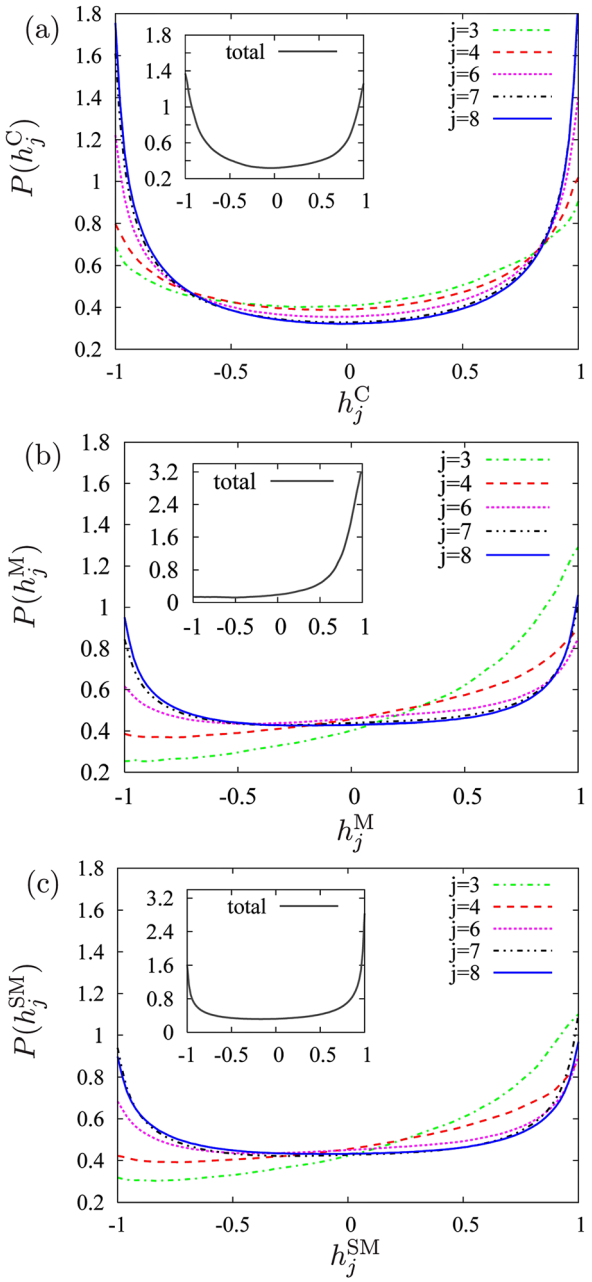

FIG. 5. (Color online) Scale-dependent PDFs of the relative helicities; (a) h_j^{C}, (b) h_j^{M}, and (c) h_j^{SM}. The insets show the PDFs of the corresponding total relative helicities.

Different types of scale-dependent dynamic alignment were found in analyses of solar wind data[14] as well as in DNS data of incompressible MHD turbulence in the presence of a strong large-scale external magnetic field.[15,16] In Ref. 14, it was shown that magnetic fluctuations in the plane perpendicular to the imposed magnetic field are more aligned/anti-aligned with the velocity being perpendicular to the imposed field, as scale decreases. In Refs. 15 and 16, Mason *et al.* confirmed the theory proposed by Boldyrev[46,47] stating that magnetic fluctuations in the plane perpendicular to the imposed magnetic field are more aligned with velocity perpendicular to the imposed field, as scale decreases within the inertial subrange, and that increasing the degree of the dynamic alignment with deceasing scale leads to scale-dependent depletion of the nonlinear interaction.

Dynamic alignment of total velocity and magnetic fields has been studied since the beginning of 1980s.[6–8] Global dynamic alignment competes with other MHD relaxation processes and has been observed in different flow configurations, like in 2D decaying MHD flows either in periodic[10] or confined domains[12] and also in 3D decaying MHD turbulence in a periodic box.[11] The degree of the alignment after many large eddy turnover times depends on initial integral quantities, i.e., the kinetic and magnetic energies and the cross and magnetic helicities. DNS of the 3D MHD turbulence showed that the local dynamic alignment occurs rapidly and is robust.[13]

Figure 5(b) shows that the distributions of the relative scale-dependent magnetic helicity h_j^{M} become more symmetric at small scales. The PDFs of h_j^{M} exhibit higher peaks at $h_j^{\mathrm{M}} = \pm 1$, as scale decreases. We also observe that the PDF of the relative total magnetic helicity is skewed, and it has a strong peak at $+1$, owing to substantial $\bar{H}^{\mathrm{M}}$ (see the inset of Fig. 5(b)).

Figure 5(c) shows that the PDFs of the relative scale-dependent super-magnetic helicity h_j^{SM} become less skewed, as scale becomes smaller. The degree of the skewness of h_j^{SM} is smaller than that of h_j^{M} at each scale. The scale-dependence of the two peaks at $h_j^{\mathrm{SM}} = \pm 1$ is the same as that for the case of h_j^{K}. The total PDF is skewed (see inset, Fig. 5(c)). However, it has two strong peaks at ± 1 corresponding to large probabilities of alignment or anti-alignment between the magnetic field $\boldsymbol{b}$ and the current density field $\boldsymbol{j}$, in contrast to the total PDF of the magnetic helicity h^{M}. The peak at $h^{\mathrm{SM}} = 1$ is higher than that at $h^{\mathrm{SM}} = -1$.

Comparing Figs. 4 and 5, it can be concluded that the scale-dependent velocity and magnetic fields are more aligned with each other, than the other vector fields studied here.

C. Eulerian and Lagrangian time-derivatives

To get further insight into the dynamics of MHD turbulence, we now analyze the Eulerian and Lagrangian accelerations defined as

$$\boldsymbol{a}^E = -(\boldsymbol{u}\cdot\nabla)\boldsymbol{u} - \frac{1}{\rho_0}\nabla P + \boldsymbol{j}\times\boldsymbol{b} + \nu\nabla^2\boldsymbol{u}, \tag{19}$$

$$\boldsymbol{a}^L = -\frac{1}{\rho_0}\nabla P + \boldsymbol{j}\times\boldsymbol{b} + \nu\nabla^2\boldsymbol{u}, \tag{20}$$

respectively. Here, we drop the forcing term $\boldsymbol{f}$, because it was only imposed at large scale and hence does not change their small-scale statistics.

In Fig. 6, we observe for MHD turbulence that the tails of the scale-dependent PDFs of the Eulerian acceleration, $\boldsymbol{a}_j^E$, and those of the Lagrangian acceleration, $\boldsymbol{a}_j^L$, become heavier, for decreasing scale. The tails of $\boldsymbol{a}_j^L$ are as heavy as $\boldsymbol{a}_j^E$ at each scale except $k_j\eta_{\mathrm{IK}} \sim 1.73 (j=8)$ where the latter is heavier than the former. We find that the tails of the PDF of the total Eulerian acceleration $\boldsymbol{a}^E$ decay more slowly than the total Lagrangian acceleration $\boldsymbol{a}^L$, which means that the former is more intermittent than the latter. This is in contrast to HD turbulence. As shown in the insets of Figs. 6(a) and 6(b),

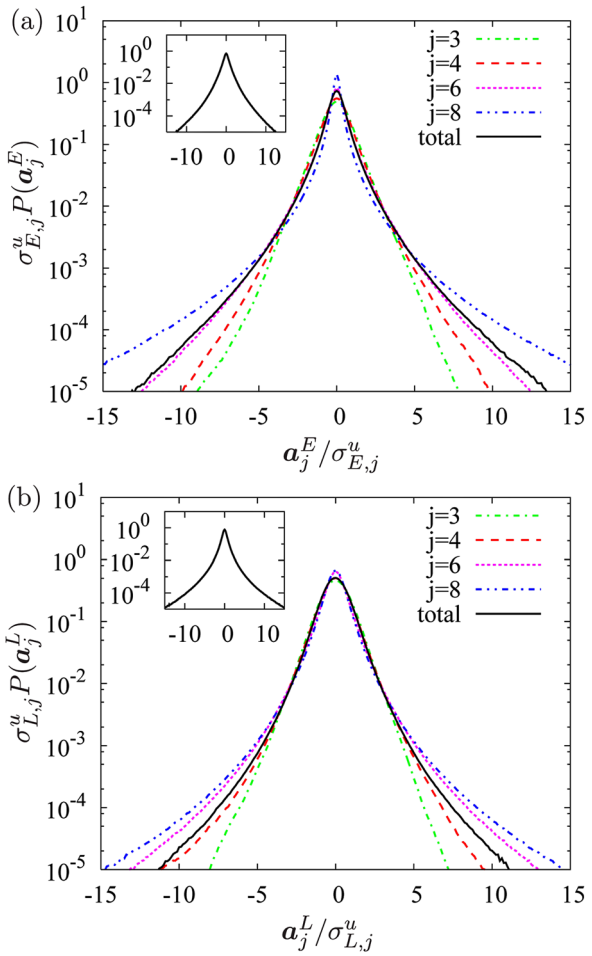

FIG. 6. (Color online) Scale-dependent PDFs of (a) the Eulerian acceleration $\boldsymbol{a}^E_j$ and (b) the Lagrangian acceleration $\boldsymbol{a}^L_j$ for MHD turbulence, where $\sigma^u_{E,j}$ and $\sigma^u_{L,j}$ are the standard deviations of $\boldsymbol{a}^E_j$ and $\boldsymbol{a}^L_j$, respectively. The insets of (a) and (b) show the PDFs of the total Eulerian and Lagrangian accelerations for HD turbulence, respectively.

the total Lagrangian acceleration shows stronger intermittency compared to the total Eulerian acceleration (e.g., Ref. 45). For a review on Lagrangian acceleration in HD turbulence, we refer to Ref. 48.

In Fig. 7, we see that the scale-dependent flatness $F[\boldsymbol{a}^L_j]$ is comparable to $F[\boldsymbol{a}^E_j]$ for $k_j\eta_{\rm IK} \lesssim 0.865 (j \leq 7)$ and that at the smallest scale, $j=8$, the former is smaller than the latter. The scale-dependent flatness $F[\boldsymbol{a}^E_j]$ increases up to 80, as scale decreases. On the other hand, the scale-dependent flatness $F[\boldsymbol{a}^L_j]$ increases up to 40 for $j \leq 7$ and then only slightly changes from $j=7$ to $j=8$. Therefore, the Lagrangian acceleration does not exhibit substantially stronger intermittency than the Eulerian acceleration, which is in contrast to HD turbulence, where the Lagrangian acceleration is much more intermittent than the Eulerian one (see inset, Fig. 7). For HD turbulence at higher $R^u_\lambda (= 732)$, it was shown that the former even exhibits extreme intermittency compared to the latter.[29] The nonlinear convection term $(\boldsymbol{u}\cdot\bigtriangledown)\boldsymbol{u}$ substantially weakens the intermittency of the Eulerian acceleration in HD turbulence, whereas this is not the case for MHD turbulence. In MHD turbulence, $(\boldsymbol{u}\cdot\bigtriangledown)\boldsymbol{u}$ does not contribute significantly to the flow intermittency except at scale $j=8$. The Lorentz force $\boldsymbol{j}\times\boldsymbol{b}$ plays a key role for the intermittency of both accelerations.

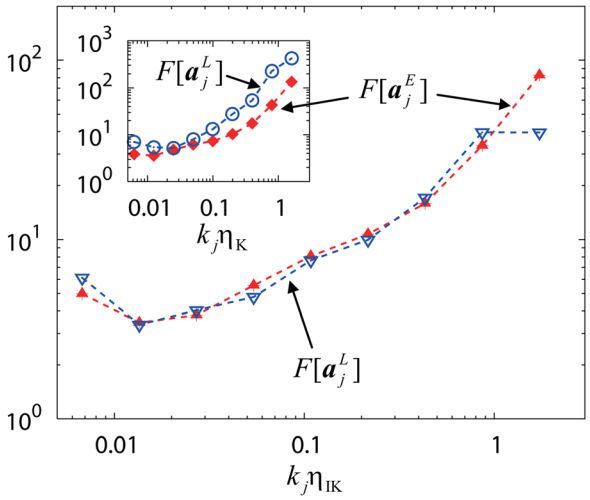

FIG. 7. (Color online) Scale-dependent flatness of the Eulerian and Lagrangian accelerations, $F[\boldsymbol{a}^E_j]$ and $F[\boldsymbol{a}^L_j]$, vs. $k_j\eta_{\rm IK}$ for MHD turbulence. The inset shows the corresponding quantities for HD turbulence.

Finally, we analyze the Eulerian and Lagrangian time-derivatives of the magnetic field, $\partial_t\boldsymbol{b}$ and $D_t\boldsymbol{b}$, in analogy to the Eulerian and Lagrangian accelerations. Here, we use the notation $D_t\boldsymbol{b} = \partial_t\boldsymbol{b} + (\boldsymbol{u}\cdot\bigtriangledown)\boldsymbol{b}$. Figure 8 illustrates that the

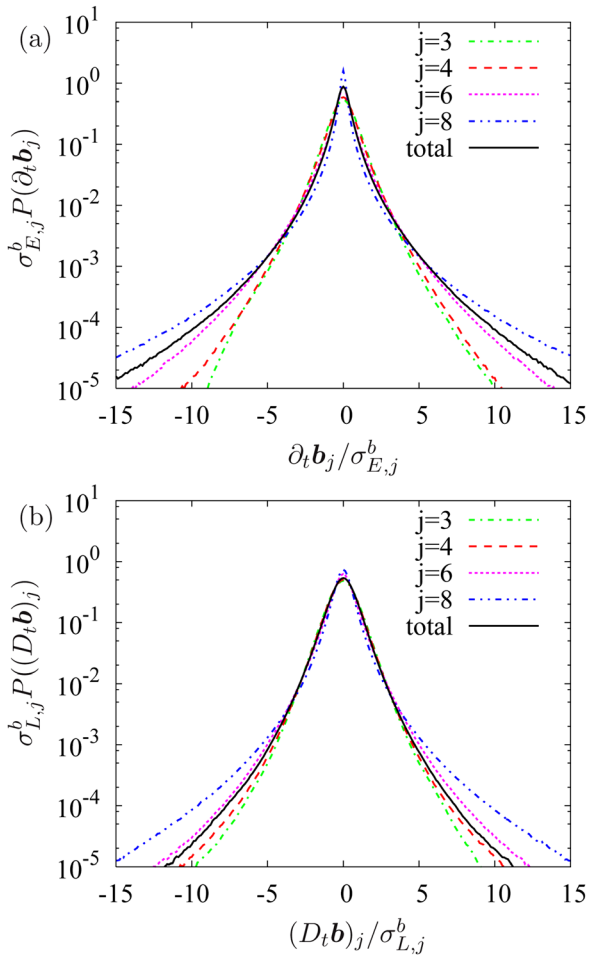

FIG. 8. (Color online) Scale-dependent PDFs of (a) the Eulerian time-derivatives of the magnetic field $\partial_t\boldsymbol{b}_j$ and (b) the Lagrangian time-derivatives of the magnetic field $(D_t\boldsymbol{b})_j$ for MHD turbulence, where $\sigma^b_{E,j}$ and $\sigma^b_{L,j}$ are the standard deviations of $\partial_t\boldsymbol{b}_j$ and $(D_t\boldsymbol{b})_j$, respectively.

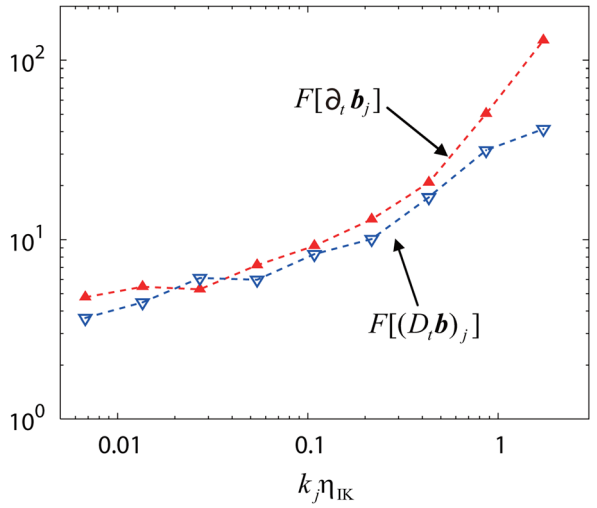

FIG. 9. (Color online) Scale-dependent flatness of the Eulerian and Lagrangian time-derivatives of the magnetic field, $F[\partial_t \boldsymbol{b}_j]$ and $F[(D_t \boldsymbol{b})_j]$, vs. $k_j\eta_{IK}$.

PDF of the total Eulerian time-derivative of the magnetic field $\partial_t \boldsymbol{b}$ exhibits heavier tails than the PDF of the total Lagrangian time-derivative $D_t \boldsymbol{b}$. The tails of the corresponding scale-dependent PDFs become heavier, as j increases.

We again assess their intermittency by considering the scale-dependent flatness of $\partial_t \boldsymbol{b}_j$ and $(D_t \boldsymbol{b})_j$ denoted by $F[\partial_t \boldsymbol{b}_j]$ and $F[(D_t \boldsymbol{b})_j]$, respectively. Figure 9 shows that $F[\partial_t \boldsymbol{b}_j] > F[(D_t \boldsymbol{b})_j]$ for scales $j \geq 3$. Therefore, we can conclude that $\partial_t \boldsymbol{b}$ is more intermittent than $D_t \boldsymbol{b}$. The convection term $(\boldsymbol{u} \cdot \nabla)\boldsymbol{b}$ thus enhances the intermittency of the Eulerian time-derivative compared to the Lagrangian one.

Comparison of Figs. 7 and 9 shows that the Eulerian time-derivative of the magnetic field $\boldsymbol{b}$ is more intermittent than the velocity $\boldsymbol{u}$ at each scale. This is consistent with the stronger intermittency of the magnetic field compared to the velocity, as quantified in Fig. 3. In contrast, the degree of the intermittency of $(D_t \boldsymbol{b})_j$ is comparable to that of $\boldsymbol{a}_j^L$.

V. CONCLUSIONS

We have examined geometrical and scale-dependent statistics to analyze the intermittency of 3D incompressible homogeneous MHD turbulence without mean magnetic field using orthogonal wavelets. The wavelet decomposition provides an ideal tool to perform scale-dependent statistics in a proper way thanks to the clear scale separation induced by the orthogonality of the basis functions. The spatial localization of wavelets allows furthermore to study the spatial variability of the statistics at a given scale, and thus yields adequate measures to quantify the intermittency of flow fields. Wavelet analysis has been applied to DNS data of MHD turbulence at $R_\lambda^u = 150$, which was computed at 512^3 grid points in a periodic box with a dealiased Fourier spectral method. DNS data of 3D incompressible homogeneous HD turbulence at $R_\lambda^u = 173$ (Refs. 44 and 45) were also analyzed for comparison.

The results confirmed that the magnetic field is indeed more intermittent than the velocity, reflected in a faster increase of the flatness with scale. Multiscale measures to study geometrical statistics, the relative scale-dependent cross and magnetic helicities together with the super-magnetic helicity, have been introduced, in addition to the relative scale-dependent kinetic helicity. We observed a higher probability for velocity and vorticity vectors to be aligned or anti-aligned, i.e., helical flow, at small scales for MHD turbulence. In contrast, the PDF of relative kinetic helicity for HD turbulence shows a higher probability for the vorticity and velocity vectors to be orthogonal at scales $k_j\eta_K \sim 0.05$ and 0.1, while the flow is helical at smaller scales $k_j\eta_K \gtrsim 0.4$. It was shown that the relative cross helicities become more pronounced at ± 1, corresponding to alignment and anti-alignment, as scale decreases. We found that the alignment or anti-alignment of the scale-dependent velocity and magnetic field, i.e., the scale-dependent dynamic alignment, is more pronounced than that of the other vectors studied here, i.e., alignment of velocity and vorticity, alignment of magnetic field and its vector potential, and alignment of magnetic field and current density, at each scale.

Finally, we examined scale-dependent statistics of the Eulerian and Lagrangian accelerations, and the corresponding time-derivatives of the magnetic field. We showed the different dynamics of MHD compared to HD turbulent flows. In MHD turbulence, the degree of intermittency of the Lagrangian acceleration is at most comparable to that of the Eulerian acceleration. In contrast, in HD turbulence, the Lagrangian acceleration exhibits substantially stronger intermittency than the Eulerian one. We also studied the Eulerian time-derivative of the magnetic field and showed that it is more intermittent than the corresponding Lagrangian time-derivative. These findings suggest that the type of intermittency in MHD turbulence is inherently different from that in HD turbulence at least for the case studied here, i.e., the case where at large scale the magnetic energy spectrum is comparable to the one of kinetic energy. We conjecture that the larger scale magnetic field, which cannot be removed from the system by transformation into any moving reference frame, contributes to the weakening of the degree of intermittency of the Lagrangian time derivatives of velocity and magnetic field compared to HD turbulence.

We have shown that the scale-dependent dynamic alignment in MHD turbulence without mean magnetic field becomes more pronounced as scale decreases up to the dissipative range. One might think that the scale-dependent dynamic alignment leads to a scale-dependent depletion of the nonlinear interaction, if one follows arguments from Boldyrev's theory[46,47] for MHD turbulence with strong mean magnetic field in the inertial subrange. Studying how the scale-dependent dynamical alignment relates to the scale-dependent depletion of nonlinearity, not only in scale, but also in space, would be intriguing, but this is beyond the scope of the present work.

In future work, it would be also interesting to examine the Reynolds number dependence of the statistics studied here. The investigation of anisotropic MHD turbulence in the presence of an imposed mean magnetic field using directional and scale-dependent statistics introduced in Ref. 37, and application of the methodology developed here to 2D MHD turbulence are other directions for further studies.

ACKNOWLEDGMENTS

The computations were carried out on the FX1 system at the Information Technology Center of Nagoya University and the HITACHI SR16000 system "Plasma Simulator" at National Institute for Fusion Science. This work was performed with the support and under the auspices of the NIFS Collaboration Research program (NIFS09KTBL012). The authors express their thanks to T. Ishihara for providing us with the DNS data of HD turbulence. K.Y. was supported by a Grant-in-Aid for Young Scientists (B) 22740255 from the Ministry of Education, Culture, Sports, Science and Technology. M.F. and K.S. thankfully acknowledge financial support from the PEPS program of INSMI-CNRS and also thank the Association CEA-EURATOM and the FRF2S (French Research Federation for Fusion Studies) for supporting their work within the framework of the EFDA (European Fusion Development Agreement) under contract V.3258.001. We also thankfully acknowledge the CIRM, Luminy, for hospitality during the 2010 CEMRACS summer program on "Numerical modeling of fusion."

[1]M. L. Goldstein, D. A. Roberts, and W. H. Matthaeus, Annu. Rev. Astron. Astrophys. **33**, 283 (1995).
[2]A. Brandenburg and K. Subramanian, Phys. Rep. **417**, 1 (2005).
[3]A. Gailitis, O. Lielausis, S. Dementév, E. Platacis, and A. Cifersons, Phys. Rev. Lett. **84**, 4365 (2000).
[4]R. Stieglitz and U. Müller, Phys. Fluids **13**, 561 (2001).
[5]R. Monchaux, M. Berhanu, M. Bourgoin, M. Moulin, Ph. Odier, J.-F. Pinton, R. Volk, S. Fauve, N. Mordant, F. Pétrélis, A. Chiffaudel, F. Daviaud, B. Dubrulle, C. Gasquet, L. Marié, and F. Ravelet, Phys. Rev. Lett. **98**, 044502 (2007).
[6]M. Dobrowolny, A. Mangeney, and P. Veltri, Phys. Rev. Lett. **45**, 144 (1980).
[7]R. Grappin, U. Frisch, J. Léorat, and A. Pouquet, Astron. Astrophys. **105**, 6 (1982).
[8]W. H. Matthaeus, M. Goldstein, and D. Montgomery, Phys. Rev. Lett. **51**, 1484 (1983).
[9]A. Pouquet, M. Meneguzzi, and U. Frisch, Phys. Rev. A **33**, 4266 (1986).
[10]A. C. Ting, W. H. Matthaeus, and D. Montgomery, Phys. Fluids **29**, 3261 (1986).
[11]T. Stribling and W. H. Matthaeus, Phys. Fluids B **3**, 1848 (1991).
[12]S. Neffaa, W. J. T. Bos, and K. Schneider, Phys. Plasmas **15**, 092304 (2008).
[13]W. H. Matthaeus, A. Pouquet, P. D. Mininni, P. Dmitruk, and B. Breech, Phys. Rev. Lett. **100**, 085003 (2008).
[14]J. J. Podesta, B. D. G. Chandran, A. Bhattacharjee, D. A. Roberts, and M. L. Goldstein, J. Geophys. Res. **114**, A01107, doi:10.1029/2008JA013504 (2009).
[15]J. Mason, F. Cattaneo, and S. Boldyrev, Phys. Rev. Lett. **97**, 255002 (2006).
[16]J. Mason, F. Cattaneo, and S. Boldyrev, Phys. Rev. E **77**, 036403 (2006).
[17]S. Servidio, W. H. Matthaeus, and P. Dmitruk, Phys. Rev. Lett. **100**, 095005 (2008).
[18]P. D. Mininni, Annu. Rev. Fluid Mech. **43**, 377 (2011).
[19]H. Politano and A. Pouquet, Phys. Rev. E **52**, 636 (1995).
[20]G. K. Batchelor and A. A. Townsend, Proc. R. Soc. London Ser. A **199**, 238 (1949).
[21]U. Frisch, *Turbulence* (Cambridge University Press, Cambridge, UK, 1995).
[22]D. Biskamp, *Magnetohydrodynamic Turbulence* (Cambridge University Press, Cambridge, UK, 2003).
[23]M. K. Verma, Phys. Rep. **401**, 229 (2004).
[24]P. D. Mininni and A. Pouquet, Phys. Rev. Lett. **99**, 254502 (2007).
[25]H. Homann, R. Grauer, A. Busse, and W. C. Müller, J. Plasma Phys. **73**, 821 (2007).
[26]H. Homann, O. Kamps, R. Friedrich, and R. Grauer, New J. Phys. **11**, 073020 (2009).
[27]J. Cho, A. Lazarian, and E. T. Vishniac, Astrophys. J. **595**, 812 (2003).
[28]N. E. Haugen, A. Brandenburg, and W. Dobler, Phys. Rev. E **70**, 016308 (2004).
[29]K. Yoshimatsu, N. Okamoto, K. Schneider, Y. Kaneda, and M. Farge, Phys. Rev. E **79**, 026303 (2009).
[30]K. Schneider, M. Farge, and N. Kevlahan, *Woods Hole Mathematics, Perspectives in Mathematics and Physics*, edited by N. Tongring and R. C. Penner (World Scientific, Singapore, 2004), Vol. 34, p. 302.
[31]M. Farge, Annu. Rev. Fluid Mech. **24**, 395 (1992).
[32]C. Meneveau, J. Fluid Mech. **232**, 469 (1991).
[33]M. Yamada and K. Ohkitani, Fluid Dyn. Res. **8**, 101 (1991).
[34]K. Schneider and O. Vasilyev, Annu. Rev. Fluid Mech. **42**, 473 (2010).
[35]K. Yoshimatsu, Y, Kondo, K. Schneider, N. Okamoto, H. Hagiwara, and M. Farge, Phys. Plasmas **16**, 082306 (2009).
[36]S. Mallat, *A Wavelet Tour of Signal Processing* (Academic, New York, 1998).
[37]W. J. T. Bos, L. Liechtenstein, and K. Schneider, Phys. Rev. E **76**, 046310 (2007).
[38]R. B. Pelz, L. Shtilman, and A. Tsinober, Phys. Fluids **29**, 3506 (1986).
[39]M. M. Rogers and P. Moin, Phys. Fluids **30**, 2662 (1987).
[40]R. M. Kerr, Phys. Rev. Lett. **59**, 783 (1987).
[41]H. K. Moffatt and A. Tsinober, Annu. Rev. Fluid Mech. **24**, 281 (1992).
[42]B. Galanti and A. Tsinober, Phys. Lett. A **352**, 141 (2006).
[43]K. Yoshida and T. Arimitsu, Phys. Fluids **19**, 045106 (2007).
[44]Y. Kaneda, T. Ishihara, M. Yokokawa, K. Itakura, and A. Uno, Phys. Fluids **15**, L21 (2003).
[45]T. Ishihara, Y. Kaneda, M. Yokokawa, K. Itakura, and A. Uno, J. Fluid Mech. **592**, 335 (2007).
[46]S. Boldyrev, Astrophys. J. **626**, L37 (2005).
[47]S. Boldyrev, Phys. Rev. Lett. **96**, 115002 (2006).
[48]F. Toschi and E. Bodenschatz, Annu. Rev. Fluid Mech. **41**, 375 (2009).